



# The characteristic of strontium-site deficient perovskites $\text{Sr}_x\text{Fe}_{1.5}\text{Mo}_{0.5}\text{O}_{6-\delta}$ ( $x = 1.9\text{--}2.0$ ) as intermediate-temperature solid oxide fuel cell cathodes

Guoquan Yang, Jie Feng, Wang Sun, Ningning Dai, Mingyue Hou, Xiaoming Hao,  
Jinshuo Qiao\*, Kening Sun\*

School of Chemical Engineering and Environment, Beijing Institute of Technology, Beijing 100081, China



## HIGHLIGHTS

- Investigation on nanostructure and performance of A-site deficient SFM materials as IT-SOFC cathodes.
- $\text{Sr}_{1.950}\text{FM}$  cathode exhibits the lowest  $R_p$  of  $0.1597 \Omega \text{ cm}^2$  at  $800^\circ\text{C}$ .
- Significantly improved power performance of cell with Sr-deficient SFM cathodes.

## ARTICLE INFO

### Article history:

Received 4 May 2014

Received in revised form

23 June 2014

Accepted 24 June 2014

Available online 7 July 2014

### Keywords:

A-site deficiency

Solid oxide fuel cell

Perovskite

Scandium-stabilized zirconium

## ABSTRACT

As the cathodes for intermediate-temperature solid oxide fuel cells (IT-SOFCs), A-site deficient  $\text{Sr}_x\text{Fe}_{1.5}\text{Mo}_{0.5}\text{O}_{6-\delta}$  ( $x = 1.9\text{--}2.0$ ) ( $\text{S}_x\text{FM}$ ) materials have been successfully synthesized using the sol–gel combustion method. In the perovskite structure of these oxides, the unit cell varies from pseudocubic to cubic with increasing deficiency. Thermal expansion coefficient of  $\text{S}_x\text{FM}$  has also been measured and compared with that of Scandium-stabilized zirconium (ScSZ) electrolyte. X-ray photoelectron spectroscopy (XPS) results indicate that the Sr-deficiency has changed the proportion of  $\text{Fe}^{2+}/\text{Fe}^{3+}$  and  $\text{Mo}^{6+}/\text{Mo}^{5+}$  ratios, which directly influences the conductivity of  $\text{S}_x\text{FM}$  materials.  $\text{S}_{1.950}\text{FM}$  possesses the largest electrical conductivity and the lowest polarization resistance ( $R_p$ ) among all the samples. The maximum power densities of a single cell with the  $\text{S}_{1.950}\text{FM}$  cathode reaches  $1083 \text{ mW cm}^{-2}$ , and the area specific resistance value is  $0.17 \Omega \text{ cm}^2$  at  $800^\circ\text{C}$ . These results indicate that the A-site deficiency could promote the electrochemical performance of SFM materials as cathodes for IT-SOFCs.

© 2014 Elsevier B.V. All rights reserved.

## 1. Introduction

With the environmental issues looms larger and the exhaustive exploitation of fossil fuels, developing new clean energy technology has aroused people's attention. The solid oxide fuel cells (SOFCs) have increasingly attracted interest as new electricity generation system due to its high energy conversion efficiency with fuel flexibility and low contamination to environment [1–4]. Lower operating temperature of  $600\text{--}800^\circ\text{C}$  can significantly diminish the premature aging of electrode materials, which could further increase the electrochemical performance of SOFCs. Therefore, the intermediate-temperature SOFCs (IT-SOFCs) is a promising research direction for SOFCs researchers [5,6]. High electrochemical

catalytic activity is necessary for the electrode materials. Some researchers reported that the electrode materials with perovskite ( $\text{ABO}_3$ ) structure could provide high oxygen reduction activities and conductivity [7,8]. At the same time, altering at A-site or B-site of the  $\text{ABO}_3$  materials can cause the nonstoichiometric of oxygen and the change of crystal structure, which further influence the electrode performance [9,10]. It is reported that the deficiency in A-site can induce the increase of oxygen vacancies and affect the concentration of cations in B-site, which contributes to changing the ionic conductivity of the  $\text{ABO}_3$  materials [11–15]. Min Jae Shin et al. has reported that the effect of oxygen transport in A-site cation deficiency in  $\text{Sr}_{1-x}\text{Fe}_{0.5}\text{Co}_{0.5}\text{O}_{3-\delta}$  ( $x = 0\text{--}0.3$ ) that Sr-deficiency enhances the stability of the perovskite structure, reduces thermal expansion at high temperatures in an Ar atmosphere, and improves the oxygen permeation fluxes [16].

$\text{Sr}_2\text{Fe}_{1.5}\text{Mo}_{0.5}\text{O}_{6-\delta}$  (SFM) with perovskite structure, has been considered as a very promising anode and cathode material for IT-

\* Corresponding authors. Tel./fax: +86 010 6891 8696.

E-mail address: [bitkengsun@163.com](mailto:bitkengsun@163.com) (K. Sun).

SOFCs because of its high electrical conductivity and electrochemical catalytic activity [17–19]. The  $\text{Fe}^{3+}/\text{Fe}^{2+}$  and  $\text{Mo}^{6+}/\text{Mo}^{5+}$  couples coexist in the cubic structure of SFM materials, and the change of chemical equilibrium of  $\text{Fe}^{3+} + \text{Mo}^{5+} \leftrightarrow \text{Fe}^{2+} + \text{Mo}^{6+}$  is closely related to the conductivity [19–22]. The substitution of elements in B-site in SFM would shift the reaction equilibrium, and therefore promote the electrical characteristics [20].

Few literature have reported the deficiency in A-site of SFM materials. Therefore, in this work, A-site cation deficient perovskite  $\text{Sr}_x\text{Fe}_{1.5}\text{Mo}_{0.5}\text{O}_{6-\delta}$  (SFM) ( $x = 2.000, 1.975, 1.950, 1.925, 1.900$ ) powders were synthesized by one-step sol-gel combustion method. The crystal structure and microstructure of the A-site deficient materials were characterized with X-ray diffraction (XRD) and scanning electron microscopy (SEM), respectively. In order to investigate the influence on the cations of B-site caused by A-site deficiency, the SFM powders were analyzed by X-ray photoelectron spectroscopy (XPS). Moreover, the electrical performances were further studied, including conductivity, electrochemical impedance spectroscopy (EIS) and the electrochemical performance.

## 2. Experimental

### 2.1. Electrode materials preparation and characterization

The powders of A-site deficient SFM perovskites in this work were synthesized by one-step sol-gel combustion method [19]. The starting materials of synthesis were  $\text{Sr}(\text{NO}_3)_2$ ,  $\text{Fe}(\text{NO}_3)_3 \cdot 9\text{H}_2\text{O}$  and  $(\text{NH}_4)_6\text{Mo}_7\text{O}_{24} \cdot 4\text{H}_2\text{O}$ . Glycine and citric acid were also used to assist the combustion. After combustion, the precursors were then calcined at 1050 °C in air for 5 h.

Other materials used in this work are 11% Scandium-stabilized zirconium (11ScSZ, Tosoh Co., Japan), 8%  $\text{Y}_2\text{O}_3$ -stabilized  $\text{ZrO}_2$  (8YSZ, Tosoh Co., Japan),  $\text{Sm}_{0.2}\text{Ce}_{0.8}\text{O}_{1.95}$  (SDC) (Fuel cell materials Co., USA) and  $\text{NiO}$  (High Purity Chemicals, Japan). For the thermal expansion coefficient (TEC) and the electronic conductivity ( $\sigma$ ) measurements, the SFM powers were pressed into a rectangular bar with a size of  $25 \times 5 \times 5 \text{ mm}^3$  under a pressure of 200 MPa, and then sintered at 1200 °C for 5 h in air.

### 2.2. Characterization of SFM powders

The phase structure of the Sr-deficient SFM materials was characterized by X-ray diffraction (XRD) (X'Pert PRO MPD). A scanning electron microscope (SEM, FEI QUANTA-250) was used to observe the microstructure of the as-prepared powders and the fabricated single cells. The thermal expansion coefficient (TEC) of the sintered sample bars were measured using a dilatometer (Netsch DIL 402C) at temperatures ranging from 40 to 1000 °C at a heating rate of 5 °C min<sup>-1</sup> in air. The electronic conductivity ( $\sigma$ ) of

the Sr-deficient SFM materials was measured by means of four-probe DC method.

### 2.3. Cell fabrication and electrochemical characterization

The electrochemical impedance spectra (EIS) of Sr-deficient perovskite SFM cathode was measured with symmetrical cell configured as SFM|SDC|ScSZ|SDC|SFM. The EIS was obtained by PARSTAT 2273, with amplitude of 10 mV over the frequency ranging from 10 mHz to 100 kHz. Here, the ScSZ electrolyte with 200 μm thickness was prepared by tape casting, then sintering at 1450 °C for 6 h. The  $\text{NiO}-\text{YSZ}$  anode-supported ScSZ thin electrolyte film was prepared by co-tape casting technology [3]. The green tapes were dried for 48 h at room temperature and first pre-sintered in air at 1300 °C for 2 h and then sintered in air at 1450 °C for 6 h. The thin ScSZ electrolyte was 10 μm in thickness. Then, an SDC ( $\text{Sm}_{0.2}\text{Ce}_{0.8}\text{O}_{1.95}$ ) interlayer, approximately 8 μm thick, which would prevent a chemical reaction between ScSZ and SFM producing a high impedance phase  $\text{Sr}_2\text{ZrO}_4$ , was screen-printed onto the ScSZ electrolyte and then calcined at 1400 °C for 5 h.

After that, the Sr-deficient SFM cathodes were then screen-printed onto the SDC interlayer, and sintered at 1100 °C for 2 h in air. At this point, the  $\text{NiO}-\text{YSZ}|\text{NiO}-\text{ScSZ}| \text{ScSZ}| \text{SDC}| \text{SFM}$  single cells were obtained. The current voltage curves of the cells were obtained by an Arbin Instruments tester (Fuel Cell Test System, FCTS). With ambient air as the oxidant and humidified hydrogen (3 vol%  $\text{H}_2\text{O}$ ) as the fuel at a flow rate of 50 mL min<sup>-1</sup>, the measurement of single cells were carried out at temperatures ranging from 650 to 800 °C.

## 3. Results and discussion

### 3.1. Crystal structure and phase stability

The X-ray diffraction (XRD) patterns of SFM powders after sintering at 1050 °C for 5 h in air were shown in Fig. 1(a). It can be observed that all the samples display a clearly and identically pure perovskite crystal structure, and no impurity phase is detected. The XRD patterns of SFM powders at 32.4° were magnified to observe details, as shown in Fig. 1(b). It can be seen that the XRD peak was slightly shifted towards high angle direction with the increasing of Sr-deficiency, which suggests that the unit cell shrinks. Moreover, the lattice parameters of a, b and c for SFM at room temperature calculated through XRD data are shown in Fig. 2. Although the highest intensity peaks can be fit well to the cubic space group  $\text{Pm}3\text{m}$  [19,20], the structures of SFM materials were pseudocubic [23]. And the value gap of a, b and c is widening with increasing Sr-deficiency. The value of a, b and c is the closest to the cubic system with  $x = 1.950$ . These data indicate that the appropriate Sr-

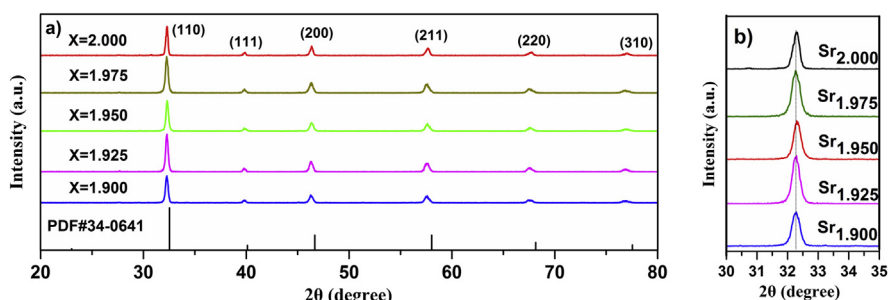
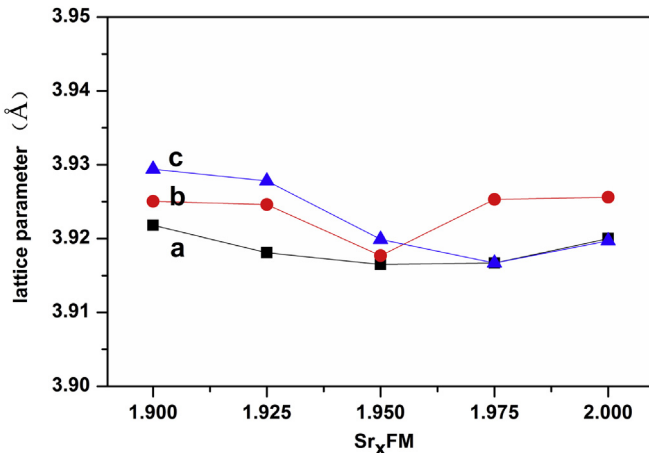


Fig. 1. X-ray diffraction patterns of Sr-deficient perovskite SFM at room temperature: (a)  $2\theta$  from 20 to 80° (b)  $2\theta$  from 30 to 35°.



**Fig. 2.** Lattice parameters of Sr-deficient perovskite SFM at room temperature.

deficiency in SFM materials may make for the change from pseudocubic to cubic perovskite.

### 3.2. Microstructure

**Fig. 3** shows the SEM images of series of Sr-deficient perovskite SFM powders. All the SFM powders have a similar overall microstructure with nanosized grains. The sponge-like porous and uniform structure with the average size of the pores of 1  $\mu\text{m}$  was obtained. The pores in the samples of  $\text{Sr}_{1.95}\text{FM}$  are obviously larger and more uniformly distributed than others, while the pores of

$\text{Sr}_{1.90}\text{FM}$  sample are most densely distributed. Parts of what makes SFM be an excellent anode or cathode material of SOFC is its porous structure, which can enlarge the triple phase boundary (TPB) of the electrodes and facilitate gas diffusion, resulting in reducing gas diffusion impedance and finally enhanced the electrochemical activity of  $\text{Sr}_{1.95}\text{FM}$  powders.

### 3.3. Thermal expansion coefficient (TEC)

The thermal expansion coefficient (TEC) is an important parameter for the electrode materials because mismatched TECs of SOFC components may result in large internal stresses and lead to cracks during fabrication and operation [14]. **Fig. 4** shows the TEC curves of SFM samples from 40 to 1000  $^{\circ}\text{C}$ .

The average TEC of SFM samples in air at the experiment temperature range were listed in **Table 1**. We can observe that different Sr-deficient ratio has a slightly influence on the TEC of the SFM oxides. The TEC value decreases to the minimum ( $14.5014 \times 10^{-6} \text{ K}^{-1}$ ) first when  $x = 1.950$  and increases then. This phenomenon may result from the crystals structure. The TEC value of SFM is somewhat higher than that of ScSZ ( $10.4 \times 10^{-6} \text{ K}^{-1}$ ). Therefore, in this work, in order to reduce the mismatch between the SFM cathode and the ScSZ electrolyte, a porous SDC ( $12.8 \times 10^{-6} \text{ K}^{-1}$ ) interlayer was introduced.

### 3.4. X-ray photoelectron spectroscopy (XPS) analysis

**Fig. 5** shows the XPS for SFM powders at room temperature, which are Mo 3d, and Fe 2p spectra, respectively. As shown in **Fig. 5(a)**, the Mo 3d spectra of SFM samples display two broad peaks

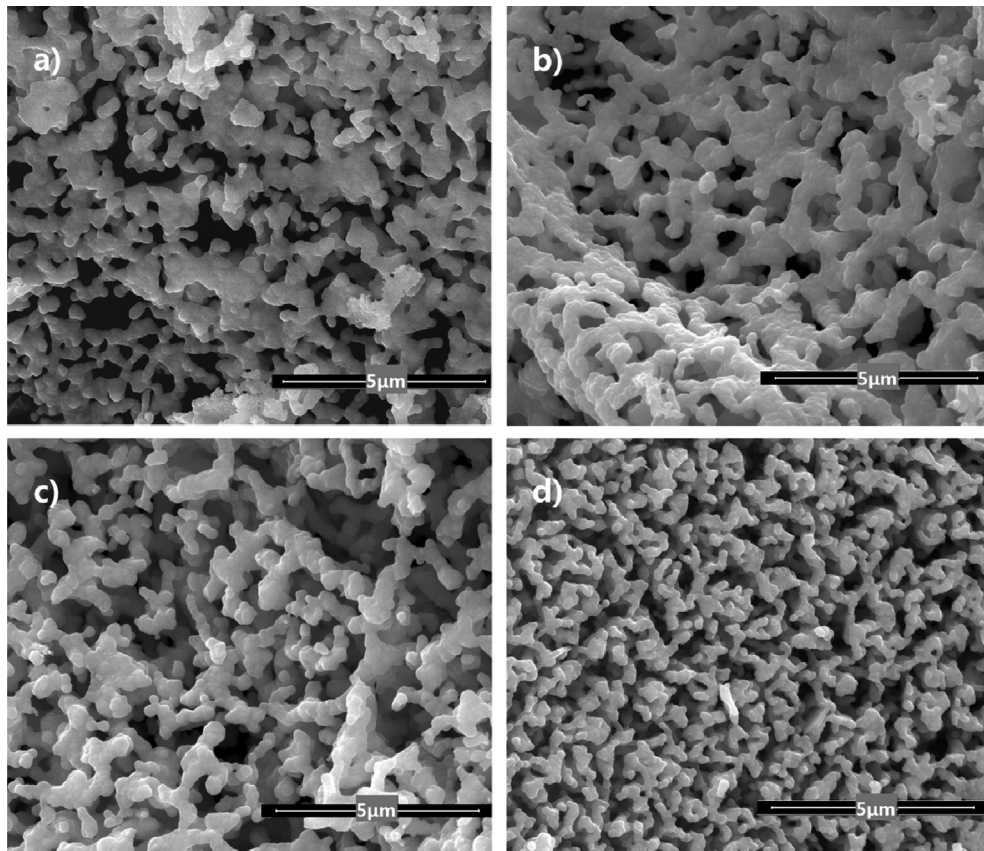


**Fig. 3.** SEM of different Sr-deficient perovskite SFM samples: a)  $\text{Sr}_{1.975}\text{FM}$ , b)  $\text{Sr}_{1.950}\text{FM}$ , c)  $\text{Sr}_{1.925}\text{FM}$ , d)  $\text{Sr}_{1.900}\text{FM}$ .

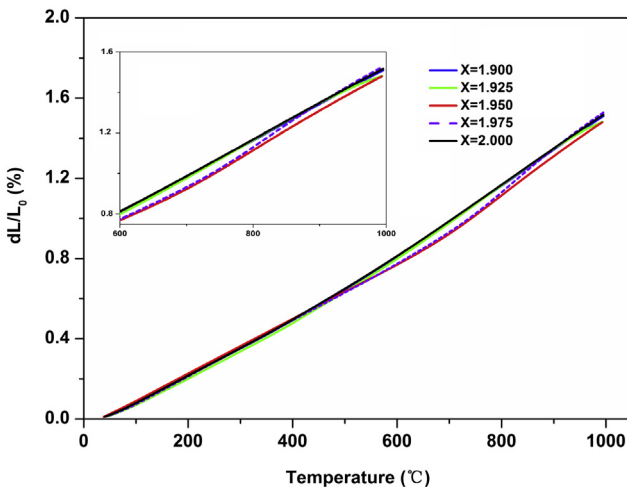


**Fig. 4.** TEC curve of series of Sr-deficient perovskite SFM samples from 40 °C to 1000 °C.

which correspond to Mo 3d<sub>5/2</sub> in the lower energy and Mo 3d<sub>3/2</sub> in the higher energy by curve fitting. It can be clearly observed that the binding energy of Mo 3d<sub>5/2</sub> around 232.1 eV and Mo 3d<sub>3/2</sub> around 235.5 eV increases with the increase of Sr deficiency, which indicates the deficiency of Sr affect the proportion of Mo<sup>6+</sup>/Mo<sup>5+</sup>. The ratio of Mo<sup>6+</sup>/Mo<sup>5+</sup> decreases to the minimum with the value of 0.45 and then increases, which is shown in Table 2.

Data analysis of Fe 2p binding energy is depicted in Fig. 5(b). As can be seen, Fe exists in mixed valence with Fe<sup>2+</sup> and Fe<sup>3+</sup> for all SFM samples. The Fe element exhibits two bands by curve fitting as

**Table 1**

The average TECs of SFM samples in the experiment temperature range from 40 °C to 1000 °C in air.

$Sr_xFe_{1.5}Mo_{0.5}O_{6-\delta}$	TEC value (40–800 °C)/ $\times 10^{-6} K^{-1}$
$x = 2.000$	14.9356
$x = 1.975$	14.7196
$x = 1.950$	14.5014
$x = 1.925$	15.1109
$x = 1.900$	15.1512

**Table 2**  
Components of Mo 3d peaks of SFM by XPS.

Samples	Mo 3d <sub>5/2</sub>		Mo 3d <sub>3/2</sub>		Mo <sup>6+</sup> /Mo <sup>5+</sup> ratio
	Mo <sup>6+</sup>	Mo <sup>5+</sup>	Mo <sup>6+</sup>	Mo <sup>5+</sup>	
$x = 2.000$	2837.44	1327.10	3585.96	3043.23	1.47
$x = 1.975$	2606.22	2535.24	2005.94	3553.65	0.76
$x = 1.950$	1812.26	3157.78	1943.42	5219.62	0.45
$x = 1.925$	2445.54	3013.61	1463.47	3445.44	0.61
$x = 1.900$	3124.87	2380.19	1578.36	2682.73	0.93

same as the Mo element. Fig. 5(b) shows that the binding energy of Fe 2p<sub>3/2</sub> around 710.4 eV shifts slightly to the low energy direction, which indicates that the deficiency of Sr has influenced the Fe element valence. Moreover, the ratio of Fe<sup>2+</sup>/Fe<sup>3+</sup> presents the same trend to Mo<sup>6+</sup>/Mo<sup>5+</sup> couple, as can be seen in Table 3.

The above XPS analysis demonstrates that the Fe<sup>2+</sup>/Fe<sup>3+</sup> and Mo<sup>6+</sup>/Mo<sup>5+</sup> couples coexist in SFM materials. And the conductivity of SFM materials is strongly subject to the chemical equilibrium of  $Fe^{3+} + Mo^{5+} \leftrightarrow Fe^{2+} + Mo^{6+}$ . When Sr-deficiency occurs, the amount of Fe<sup>3+</sup> and Mo<sup>5+</sup> will increase, as clearly shown in Fig. 5 and Tables 2 and 3. The minimum Fe<sup>2+</sup>/Fe<sup>3+</sup> ratio and Mo<sup>6+</sup>/Mo<sup>5+</sup> ratio are obtained at  $x = 1.95$  for  $Sr_xFe_{1.5}Mo_{0.5}O_{6-\delta}$ , which may contribute to increasing its electronic conductivity [20].

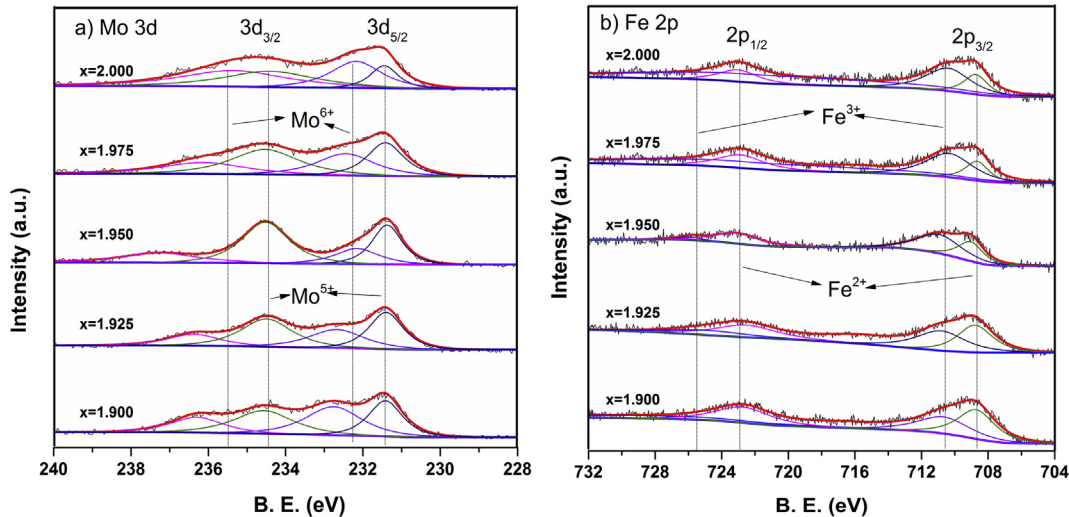
### 3.5. Electrochemical properties and performance

#### 3.5.1. Conductivities

The electronic conductivity plays an important role in total electrical conductivity for the perovskite materials. The electronic conductivity ( $\sigma$ ) of  $Sr_xFe_{1.5}Mo_{0.5}O_{6-\delta}$  ( $x = 1.900$ –2.000) samples in air from 300 to 850 °C is shown in Fig. 6. The conductivity first exhibits an increasing trend to the maximum at 550 °C, and then decreases with further increasing temperature. These results can be described using the small polaron hopping mechanism [18,24], where electron charge carriers are generated via temperature activated disproportionation reaction:



In low temperature range, the disproportionation reaction increases which induces the small polaron increasing and enhances the electrical conductivity. Oppositely, above 550 °C, the

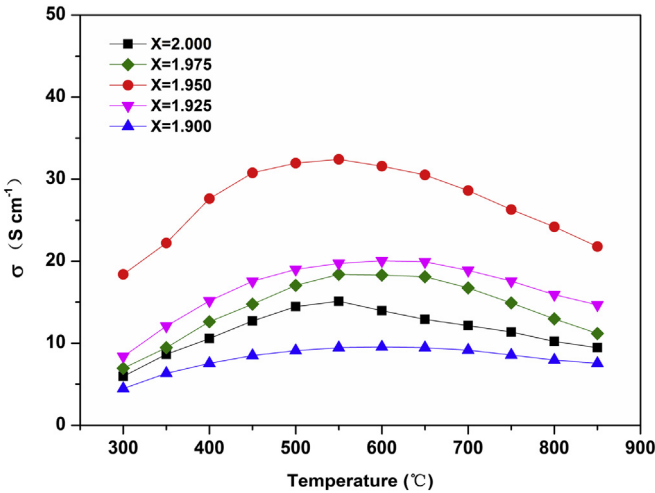


**Fig. 5.** XPS spectra at room temperature for SFM: (a) Mo 3d (b) Fe 2p.

**Table 3**

Components of Fe 2p peaks of SFM by XPS.

Samples	Fe 2P <sub>3/2</sub>		Fe 2P <sub>1/2</sub>		Fe <sup>2+</sup> /Fe <sup>3+</sup> ratio
	Fe <sup>2+</sup>	Fe <sup>3+</sup>	Fe <sup>2+</sup>	Fe <sup>3+</sup>	
X = 2.000	1688.79	3619.38	7208.18	1637.26	1.69
X = 1.975	1611.78	3971.95	6627.49	1530.28	1.49
X = 1.950	2294.02	3889.16	2237.16	320.33	1.34
X = 1.925	5090.01	3660.71	4016.96	2035.50	1.60
X = 1.900	5265.24	4066.97	7520.32	3712.82	1.64

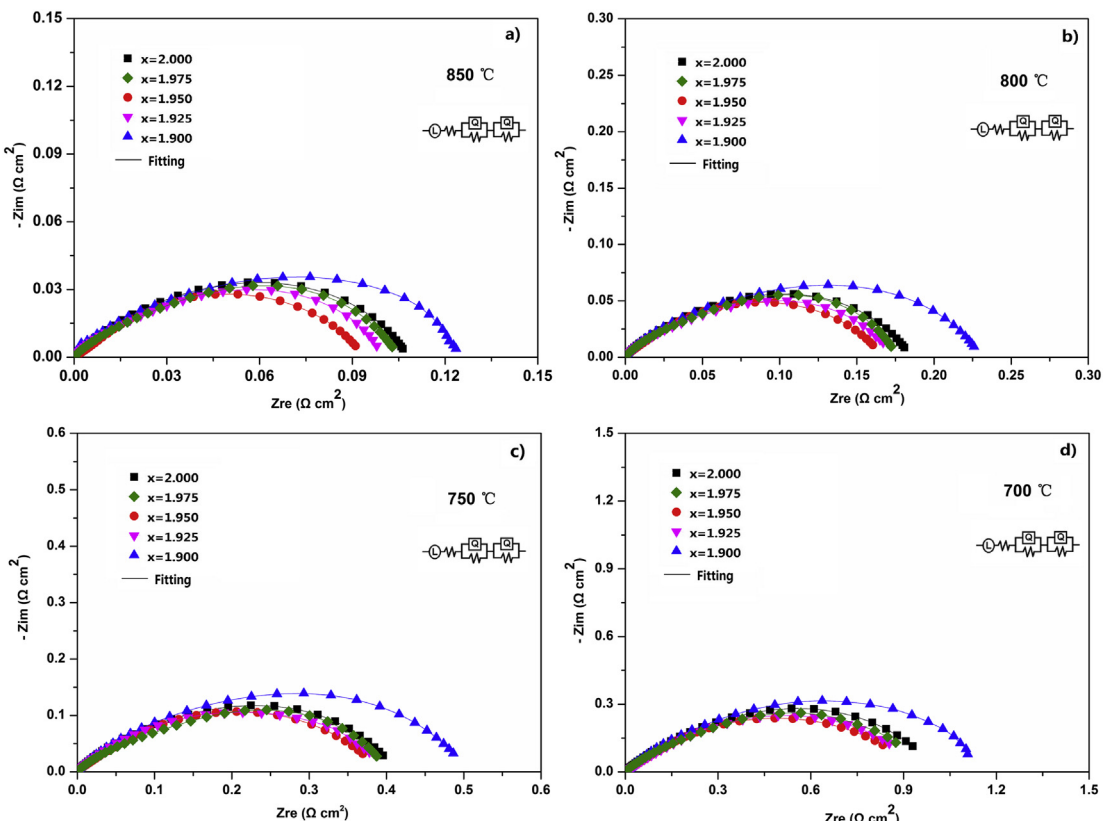
**Fig. 6.** The electronic conductivity ( $\sigma$ ) of SFM samples in air from 300 °C to 850 °C.

conductivity can be explained by the formation of oxygen vacancies. The conductivity decreases with temperature which is relevant to the lattice oxygen loss [18]. In high temperature range, the conductivity can be explained by the formation of oxygen vacancies which may act as scattering centers, or as random traps for electrons, resulting in reduce of carrier mobility [25].

For all samples, the conductivity has a sharp increase up to the maximum of 33 S cm<sup>-1</sup> at  $x = 1.950$ , and then shows a gradually decreasing trend. These results may be attributed to that the chemical equilibrium  $\text{Fe}^{3+} + \text{Mo}^{5+} \leftrightarrow \text{Fe}^{2+} + \text{Mo}^{6+}$  would shift towards to the right side with the deficiency increase [20], which has been analyzed in the previous section of XPS. This chemical equilibrium shift is favorable for the conductivity enhancement. On the other hand, oxygen vacancies variation in SFM materials, a p-type semiconductor, which is related to the Sr-site deficiency, may also account for this. More vacancies occur as Sr-site deficiency increase in the SFM materials, which enhanced the oxygen ion conductivity at some extent. However, the excess oxygen vacancies in SFM will produce the association with B-site cations, which could result in the decrease of conductivity.

### 3.5.2. EIS of Sr-site deficient perovskite cathodes

The EIS of SFM cathode were measured in atmospheric air in the temperature range of 700–850 °C and the EIS results and fitting curves of SFM cathodes were shown in Fig. 7. In the fitted with the equivalent circuit  $LR_{\Omega}(Q_{\text{H}}R_{\text{H}})(Q_{\text{L}}R_{\text{L}})$ , where  $R_{\Omega}$ ,  $R_{\text{H}}$  and  $R_{\text{L}}$  are the electrolyte ohmic, electrode polarization resistance at high and low frequency, respectively. For comparison, the ohmic resistance ( $R_{\Omega}$ ) was omitted in the Nyquist plots. The difference between the real axis intercepts of the impedance arc is considered to be the cathodic polarization resistance ( $R_{\text{p}}$ ) including  $R_{\text{H}}$  and  $R_{\text{L}}$ . The curves of the  $R_{\text{p}}$  values are shown in Fig. 8, which exhibits a

**Fig. 7.** Impedance spectra of SFM cathodes with different Sr-deficiency at (a) 850 °C, (b) 800 °C, (c) 750 °C, (d) 700 °C in air.

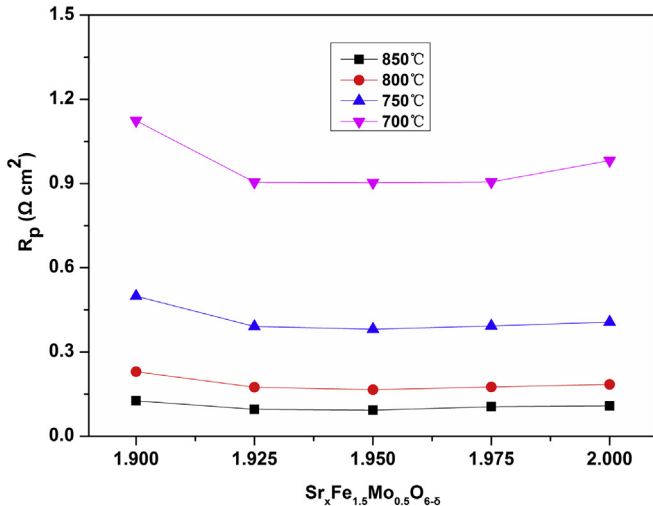


**Fig. 8.** Dependence of  $R_p$  for SFM cathodes with different Sr-deficiency at 700–850 °C in air.

decreasing trend to the minimum and then increases. It can be observed that the  $R_p$  value reaches the minimum when  $x = 1.950$  and the maximum when  $x = 1.900$ . The  $R_p$  values of  $\text{Sr}_x\text{Fe}_{1.5}\text{Mo}_{0.5}\text{O}_{6-\delta}$  ( $x = 1.900, 1.925, 1.950, 1.975, 2.000$ ) cathodes are 0.2288, 0.1750, 0.1597, 0.1638 and 0.1809  $\Omega \text{ cm}^2$  at 800 °C, respectively. The results indicate that Sr-deficient SFM cathode shows excellent performance.

The reduction reaction of oxygen not only occurs at the TPB, but will also extend to the surface and inner of the cathode materials. When the oxygen molecules are adsorbed on the surface of the cathode materials, they will be dissociated into oxygen atoms, and reduced to oxygen ions entering into the interior. As deficiency

occurs in the Sr-sites, there will be the generation of the oxygen vacancies at the surface and inner of SFM. The surface oxygen vacancies would promote the adsorption and dissociation of the oxygen molecule, while the internal oxygen vacancies provide the channel for the migration of oxygen ions. These reasons would account for the decrease of  $R_p$  as Sr-deficiency increases.

### 3.5.3. Discharge performance of the cells

**Fig. 9(a–c)** displays the  $I$ – $V$  and  $I$ – $P$  curves of NiO–YSZ|ScSZ anode-supported cells with SDC interlayer and SFM cathode, operating at 650–800 °C. The  $\text{S}_x\text{FM}$  powders of  $x = 2.000, 1.950, 1.900$  were chosen to carry on the discharge performance of the cells in this work according to EIS results (Section 3.5.2). The open circuit voltage (OCV) is over 1.0 V, which indicates that the electrolyte is sufficiently dense. As shown in **Fig. 9**, the cell with  $\text{S}_x\text{FM}$  cathodes at  $x = 2.000, 1.950, 1.900$  demonstrates maximum power densities of 896, 1083, 823  $\text{mW cm}^{-2}$  at 800 °C, respectively. These data suggest that the appropriate amount of Sr-deficiency can improve the electrical characteristics of SFM cathode.

The fuel cell impedance spectroscopy obtained under open circuit state at 800 °C was shown in **Fig. 9(d)**. The data are appropriately fitted with the equivalent circuit  $L R_\Omega (Q_\text{H} R_\text{H}) (Q_\text{I} R_\text{I})$ . The smallest ohmic resistances ( $R_\Omega$ ), which is about 0.025  $\Omega \text{ cm}^2$ , may be related to the ohmic resistance of electrode, electrolyte and the contact resistance. The polarization resistance ( $R_p$ ) differs with  $x$ , which indicates that the Sr-deficiency has an impact on the performance of cathode materials. The fitting curves display two semi-circles at different scanning frequencies. Compared with the other two cells, the cell with  $\text{S}_{1.950}\text{FM}$  cathode exhibits small semi-circle at low frequency, demonstrating low resistance of diffusion for fuel and oxygen, which is attributed to the porous microstructure. Meanwhile, the cell with  $\text{S}_{1.950}\text{FM}$  cathode also shows the most depressed semi-circle at higher frequency, indicating the lowest charge transfer resistance. This can be explained with the fact that

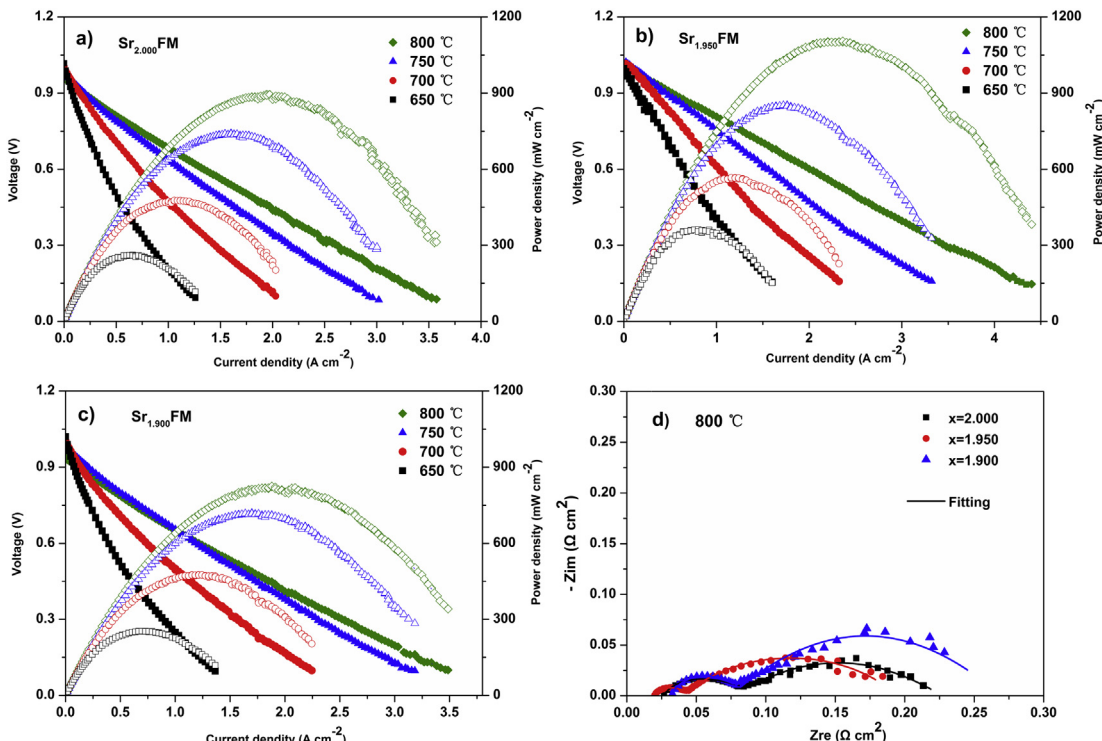


**Fig. 9.**  $I$ – $V$  and  $I$ – $P$  curves of the single cells with SFM cathode at 650–800 °C: (a)  $\text{Sr}_{2.000}\text{FM}$ , (b)  $\text{Sr}_{1.950}\text{FM}$ , (c)  $\text{Sr}_{1.900}\text{FM}$ , and (d) the EIS of the single cells at 800 °C.

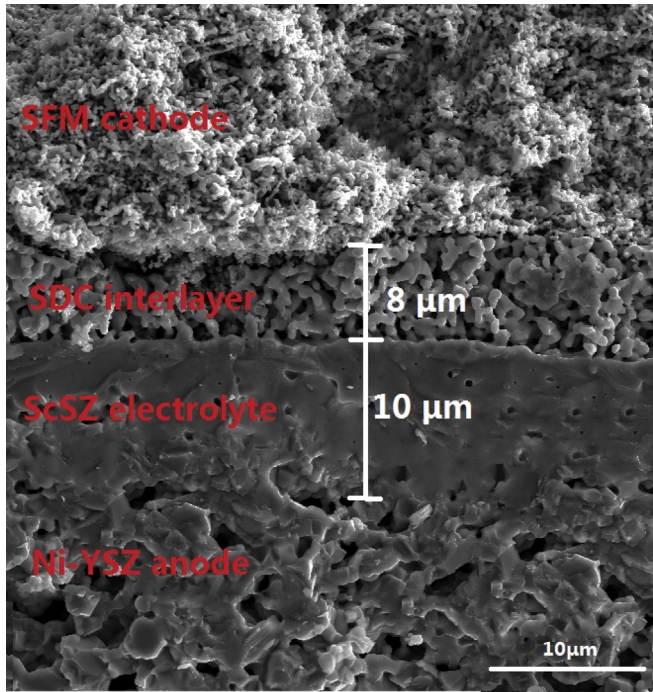


**Fig. 10.** The SEM of the fracture cross-section of single cells.

Sr-deficiency can induce much more oxygen vacancies which promote the transfer of oxygen ions.

Fig. 10 shows the SEM of the fracture cross-section of single cells. In the SEM micrograph the electrolyte and electrodes can be discerned: a highly porous Ni-YSZ anode, a dense ScSZ layer with thickness of 10  $\mu\text{m}$  adhered to the porous anode, an SDC interlayer of 8  $\mu\text{m}$  adhered to the electrolyte, and the SFM cathode of 40  $\mu\text{m}$ . It can be seen that no cracks is observed and the electrolyte film is very thin, which demonstrate that tape casting can be used to prepare high quality anode-supported SOFCs.

#### 4. Conclusions

A-site deficient  $\text{Sr}_x\text{Fe}_{1.5}\text{Mo}_{0.5}\text{O}_{6-\delta}$  ( $x = 1.900, 1.925, 1.950, 1.975, 2.000$ ) materials have been successfully synthesized using the sol–gel combustion method and studied as the cathodes for IT-SOFCs. XRD spectra confirmed the SFM powders of the perovskite structure, and that the unit cell varies from pseudocubic to cubic with increasing deficiency. The unit cell is the most approaching to cubic with  $x = 1.950$ . The Sr-deficiency with  $1.950 \leq x \leq 2.000$  reduces thermal expansion at the experiment temperature range, which is an advantage for reducing the mismatch between the cathode and electrolyte. XPS analyses reveals that the Sr-deficiency changes the proportion of  $\text{Fe}^{2+}/\text{Fe}^{3+}$  and  $\text{Mo}^{6+}/\text{Mo}^{5+}$  ratios, which induces the shift of the chemical equilibrium and results in high electrical conductivity. Consequently, the enhanced conductivity is observed in Sr-deficient samples. The electrical conductivity continuously increases to the maximum value at a characteristic temperature and then decreases with the temperature increasing.

A maximum conductivity of  $33 \text{ S cm}^{-2}$  which is an improvement when compared to  $x = 2.000$  at  $550^\circ\text{C}$  was observed with  $x = 1.950$ . Meanwhile, the EIS results exhibit that  $\text{S}_{1.950}\text{FM}$  cathode has exhibited electrochemical performance with the lowest  $R_p$  on ScSZ electrolyte among all the samples. With the deficiency of 0.050 in A-site, the maximum power densities of a single cell at  $800^\circ\text{C}$  increased from 896 to 1083  $\text{mW cm}^{-2}$  in  $\text{H}_2$ , and the area specific resistance value with  $\text{S}_{1.950}\text{FM}$  cathode is  $0.17 \Omega \text{ cm}^2$  at  $800^\circ\text{C}$ . These results suggest that the A-site deficiency can substantially improve the electrochemical performance of SFM materials for IT-SOFCs.

#### Acknowledgments

This work is financial supported by National Natural Science Foundation of China (Grant no. 21376001) and also supported by the Excellent Young Scholars Research Fund of Beijing Institute of Technology, contract no.2013YR1013.

#### References

- [1] S. Park, J.M. Vohs, R.J. Grote, *Nature* 404 (2000) 265–267.
- [2] Z.L. Zhan, S.A. Barnett, *Science* 308 (2005) 844–847.
- [3] Chengcheng Wang, Linghong Luo, Yefan Wu, bingxue Hou, Liangliang Sun, *Mater. Lett.* 65 (2011) 2251–2253.
- [4] L. Yang, C.D. Zuo, S.Z. Wang, K. Blinn, M.F. Liu, Z. Cheng, M.L. Liu, *Science* 326 (2009) 126–129.
- [5] C.H. Zhao, R.Z. Liu, L. Shao, S.R. Wang, T.L. Wen, *Electrochim. Commun.* 11 (2009) 2300–2303.
- [6] C.-W. Kwon, J.-W. Son, J.-H. Lee, H.-M. Kim, H.-W. Lee, K.-B. Kim, *Adv. Funct. Mater.* 21 (2011) 1154–1159.
- [7] G.L. Xiao, Q. Liu, F. Zhao, L. Zhang, C.R. Xia, F.L. Chen, *J. Electrochem. Soc.* 158 (2011) B455–B460.
- [8] Q. Liu, D.E. Bugaris, G.L. Xiao, M. Chmara, S.G. Ma, H.-C.Z. Loyer, M.D. Amiridis, F.L. Chen, *J. Power Sources* 196 (2011) 9148–9153.
- [9] Brendan J. Kennedy, Christopher J. Howard, Yoshiki Kubota, Kenichi Kato, *J. Solid State Chem.* 177 (2004) 4552–4556.
- [10] K.K. Hansen, K. Vels Hansen, *Solid State Ionics* 178 (2007) 1379–1384.
- [11] Anton R. Chakhmouradian, Roger H. Mitchell, Peter C. Burns, *J. Alloys Compd.* 307 (2000) 149–156.
- [12] V.V. Kharton, A.V. Kovalevsky, E.V. Tsigas, A.P. Viskup, E.N. Naumovich, J.R. Jurado, J.R. Fraile, *J. Solid State Electrochem.* 7 (2002) 30–36.
- [13] Ahmed D. Aljaberi, John T.S. Irvine, *J. Mater. Chem. A* 1 (2013) 5868–5874.
- [14] Azra Yaqub, Cristian Savaniu, Naveed K. Janjua, John T.S. Irvine, *J. Mater. Chem. A* 1 (2013) 14189–14197.
- [15] Masayoshi Yuasa, Naoki Tachibana, Kengo Shimane, *Chem. Mater.* 21 (2009) 5307–5318.
- [16] Min Jae Shin, Ji Haeng Yu, *J. Membr. Sci.* 401–402 (2012) 40–47.
- [17] Q. Liu, X.H. Dong, G.L. Xiao, F. Zhao, F.L. Chen, *Adv. Mater.* 22 (2010) 5478–5482.
- [18] Xin Pan, Zhenbin Wang, Beibei He, Shaorong Wang, Xiaojun Wu, Changrong Xia, *Int. J. Hydrogen Energy* 38 (2013) 4108–4115.
- [19] Ningning Dai, Zhongliang Lou, Zhenhua Wang, Xiaoxi Liu, Yiming Yan, Jinshuo Qiao, Taizhi Jiang, Kening Sun, *J. Power Sources* 243 (2013) 766–772.
- [20] Ningning Dai, Jie Feng, Zhenhua Wang, Taizhi Jiang, Wang Sun, Jinshuo Qiao, Kening Sun, *J. Mater. Chem. A* 1 (2013) 14147–14153.
- [21] George J. Nelson, Arata Nakajo, Brice N. Cassenti, Matthew B. DeGostin, Kyle R. Bagshawa, Aldo A. Peracchio, Guoliang Xiao, Steve Wang, Fanglin Chen, Wilson K.S. Chiu, *J. Power Sources* 246 (2014) 322–334.
- [22] Ana B. Munoz-Garcia, Michele Pavone, Andrew M. Ritzmann, Emily A. Carter, *Phys. Chem. Chem. Phys.* 15 (2013) 6250–6259.
- [23] Ana B. Munoz-Garcia, Daniel E. Bugaris, Michele Pavone, *J. Am. Chem. Soc.* 134 (2012) 6826–6833.
- [24] Junling Meng, Xiaojuan Liu, Lin Han, Yijia Bai, Chuangang Yao, Jian Meng, *J. Power Sources* 247 (2014) 845–851.
- [25] Shuyan Li, Zhe Lu, Xiqiang Huang, Wenhui Su, *Solid State Ionics* 178 (2008) 1853–1858.